The limitations of extending nature's color palette in correlated, disordered systems

Gianni Jacucci[a], Silvia Vignolini[a,1], and Lukas Schertel[a]

[a]Department of Chemistry, University of Cambridge, Cambridge CB2 1EW, United Kingdom

Edited by Lia Addadi, Weizmann Institute of Science, Rehovot, Israel, and approved August 2, 2020 (received for review May 24, 2020)

Living organisms have developed a wide range of appearances from iridescent to matte textures. Interestingly, angular-independent structural colors, where isotropy in the scattering structure is present, only produce coloration in the blue wavelength region of the visible spectrum. One might, therefore, wonder if such observation is a limitation of the architecture of the palette of materials available in nature. Here, by exploiting numerical modeling, we discuss the origin of isotropic structural colors without restriction to a specific light scattering regime. We show that high color purity and color saturation cannot be reached in isotropic short-range order structures for red hues. This conclusion holds even in the case of advanced scatterer morphologies, such as core-shell particles or inverse photonic glasses—explaining recent experimental findings reporting very poor performances of visual appearance for such systems.

structural color | correlated disorder | optical materials | disordered photonics

Structural colors are the results of constructive interference of light scattered by nanostructured, nonabsorbing media (1, 2). In contrast to color by pigmentation, where the color results from wavelength-selective absorption, structural colors spanning across the entire visible spectrum can be obtained using only one scattering material in a matrix medium (e.g., air). The possibility of exploiting such photonic coloration to replace traditional pigments catalyzed the efforts of several research groups (3–9). Structural colors come with various advantages compared to conventional pigments: 1) structural pigments do not bleach, as the color formation is defined by the architecture instead of the composition; 2) they can be constituted of environmental-friendly materials (10, 11); and 3) they achieve unconventional color effects, from vivid metallic to isotropic optical response.

Isotropic structural color is especially appealing when it comes to replacing traditional pigmentation as it preserves an angular-independent appearance. Therefore, several methods were developed to produce hierarchical (6, 12, 13) or short-range order structures with angular-independent colors (4, 14, 15). Such studies of short-range order structures, often referred to as photonic glasses (PGs), found inspiration in analogous two-dimensional (2D) structures exploited in birds (Fig. 1) (16–19). However, in nature, such PGs have been reported only to produce blue colors as green and red coloration are usually achieved with long-range ordered structures or using pigmentation (20, 21).

In the following, we investigate the limitations of color creation by scattering from disordered, short-range correlated structures. We question whether a saturated, angular-independent color response can be achieved only in the UV–blue spectral region or whether nature has missed a trick and developed other mechanisms for red hues. In fact, while artificial PGs with red hues have been reported, their optical properties are rather poor—their color saturation and purity are limited, holding these materials back from applications. These limitations of red isotropic structural color have been attributed to single-particle resonances (22). However, this conclusion ignored multiple scattering and coupling effects between particles, which are known to play a major role in PGs (14, 23). Here we exploit a numerical approach that provides direct access to the reflection spectrum of an arbitrary structure and allows us to investigate intermediate scattering regimes, i.e., in between single scattering and diffusive behavior, without further assumptions. With this method, we show that nature's solution is actually optimal for blue production only: both high- and low-refractive index contrast PGs show poor color purity in the red. We demonstrate the difficulty in achieving isotropic structural color in the red spectral region with high saturation and purity even for advanced morphologies of the scatterers in both direct and inverse PGs.

Results

Direct vs. Inverse Photonic Glasses. Photonic glasses with tailored scatterer properties (represented by the form factor in the calculation of the scattering cross-section; *SI Appendix*, Section I) and structural correlation (structure factor) were generated using a recently developed numerical algorithm; see details in ref. 25 and *SI Appendix*, Section III. The optical properties of the generated structures were then calculated using a finite difference time domain (FDTD) method. We limited our calculations to 2D structures, a case often found in natural systems (Fig. 1). The study of 2D media allows us to probe a large parameter space while limiting computational costs. Nevertheless, we believe that the same general considerations can be extended to the 3D case, as we focus on low-refractive index, weakly scattering media—conversely to highly scattering systems where phase transitions in the light transport regimes strongly depend on the dimensionality (26–34).

Significance

Scattering from 2D correlated disordered structures is often at the core of matte color appearances in nature. However, the hues related to this mechanism are restricted to UV radiation and the blue part of the visible spectrum. Here we present a numerical study on short-range correlated materials—photonic glasses—without the restriction to a specific light transport regime. We demonstrate that with these materials, saturated angle-independent structural colors cannot be reached in the long-wavelength region of the visible spectrum. In this context, we discuss promising approaches toward 3D isotropic structural colored materials.

Author contributions: G.J., S.V., and L.S. designed research; G.J. and L.S. performed research; G.J. and L.S. contributed new reagents/analytic tools; G.J. and L.S. analyzed data; and G.J., S.V., and L.S. wrote the paper.

The authors declare no competing interest.

This article is a PNAS Direct Submission.

[1]To whom correspondence may be addressed. Email: sv319@cam.ac.uk.

This article contains supporting information online at https://www.pnas.org/lookup/suppl/doi:10.1073/pnas.2010486117/-/DCSupplemental.

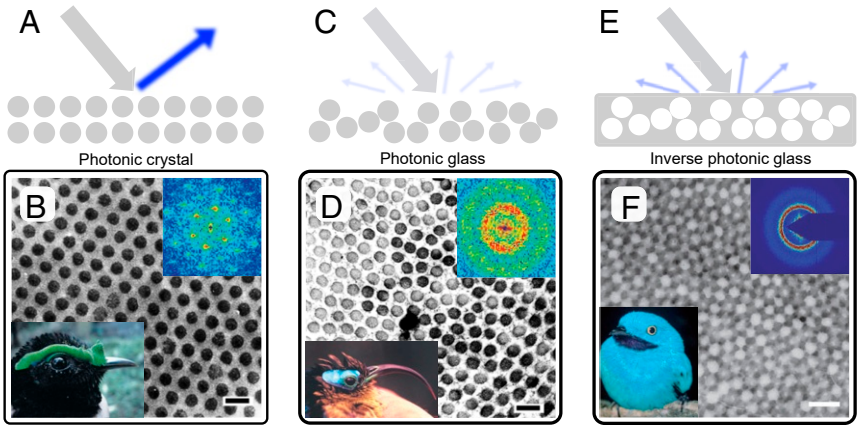

Fig. 1. Structural color in natural systems. Sketch of light scattered by (*A*) a photonic crystal, (*C*) a photonic glass, and (*E*) an inverse photonic glass. (*B*) Transmission electron micrograph of collagen arrays from structurally colored facial caruncles of male asities *Philepitta castanea* (*Lower Left Inset*) and its 2D Fourier power spectra (*Upper Right Inset*). (*D*) TEM of collagen arrays from structurally colored facial caruncles of male asities *Neodrepanis coruscans* (*Lower Left Inset*) and its 2D Fourier power spectra (*Upper Right Inset*) (17). (*B* and *D*) Adapted with permission of The Company of Biologists Ltd., from ref. 17; permission conveyed through Copyright Clearance Center, Inc. (Scale bars: 200 nm.) (*F*) EM image of sphere-type keratin and air nanostructure from back contour feather barbs of *Cotinga maynana* (*Lower Left Inset*) and corresponding small-angle X-ray scattering data (*Upper Right Inset*). Adapted with permission of the Royal Society of Chemistry, from ref. 24; permission conveyed through Copyright Clearance Center, Inc. (Scale bar: 500 nm.)

In the absence of absorption, scattering in PGs emerges from the interplay between 1) single particle properties such as size, shape, and refractive index and 2) ensemble properties such as filling fraction and structural correlations. As depicted in Fig. 2*A*, for the case of direct PGs the reflection is dominated by Mie resonances, determined by the scatterer properties. The reflected color can be, therefore, tuned in the visible by changing the scatterer dimensions. However, as the particle size increases, the Mie resonance peak red-shifts, and a second peak appears in the blue part of the spectrum, corresponding to a higher-order resonant mode (*SI Appendix*, Figs. S1 and S2). In contrast, light scattering in inverse PGs is dominated by structural correlations (Fig. 2*B*). The reflection peak, whose position corresponds well to Bragg's law predictions, is more pronounced than in direct structures. Moreover, when the structural peak is shifted at red wavelengths, the form-factor resonance at short wavelengths is less marked than in Fig. 2*A*. The occurrence of a separated peak in the visible spectrum showcases that using inverse PGs is an effective strategy to minimize the form-factor weight on the overall optical response of a system in favor of structural contributions.

The Role of Refractive Index. The dependency of isotropic structural coloration on the refractive index is shown in *SI Appendix*, Figs. S1 and S2, for direct and inverse PGs, respectively. Changing the refractive index affects the interplay between form- and structure-factor contributions. High-refractive index systems are dominated by form-factor resonances preventing them from reaching good color purity in the red spectral region, for both direct and inverse PGs. For direct systems, even when the refractive index contrast is low, form-factor resonances lead to an enhanced reflection in the short-wavelength side of the structural peak—similarly to Fig. 2*A*. In contrast, for the case of inverse PGs, we observe that the structure-factor forms a well-separated peak in the visible spectrum, even in the red wavelength region. This allows us to conclude that low-refractive index, inverse PGs can outperform their direct counterpart in terms of color purity and saturation.

Reducing the refractive index contrast between the scattering matrix (n_m) and the scattering centers (n_p) can further favor structural contributions. Fig. 3*A* shows that increasing n_p results in a broadband reduction of the reflectance and a red shift of the structural peak. Moreover, the structural peak decreases in width and has a higher intensity compared to its background, leading to better color purity. The reduction of the refractive index contrast lowers the role of multiple scattering, which is anyway present in disordered systems. This limits the isotropic structural colors to a light propagation regime in between diffusive scattering and ballistic transport. The multiple scattering becomes dominant when the sample thickness is increased, leading to a broadband unsaturated response (*SI Appendix*, Fig. S3*A*).

To further investigate the advantages and limitations of isotropic structural coloration in direct and inverse PGs, we studied their dependency on different ensemble parameters. *SI Appendix*, Fig. S3*B*, shows the optical response of inverse PGs is more robust to variations in scatterer size distribution than the direct PGs. While for direct PGs, polydispersity averages out the Mie resonances, in inverse PGs, polydispersity only slightly affects the structure-factor resonance peak. In inverse PGs, the polydispersity helps to reduce the Mie resonance intensity in

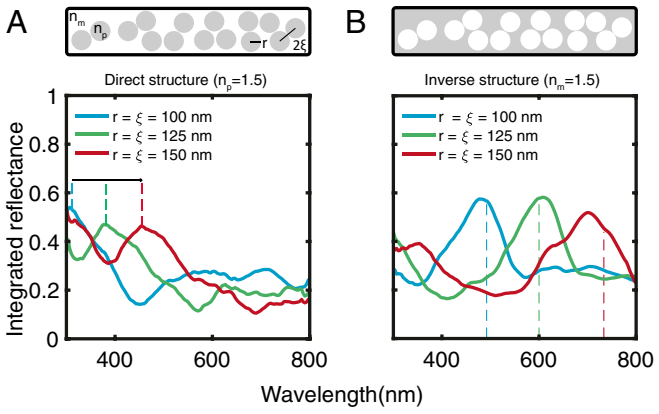

Fig. 2. Simulated optical response for (*A*) direct and (*B*) inverse photonic glasses. Inverse PGs, where scattering is dominated by structural correlations, exhibit a spectral peak whose position can be tuned over the whole visible range controlling the size of the scatterers. Dotted lines indicate the position of the first Mie resonance (form factor resonance) in direct PGs and the Bragg's law prediction (structure factor resonance) in inverse PGs. All of the simulated structures have a thickness of 3 μm and ff = 0.5.

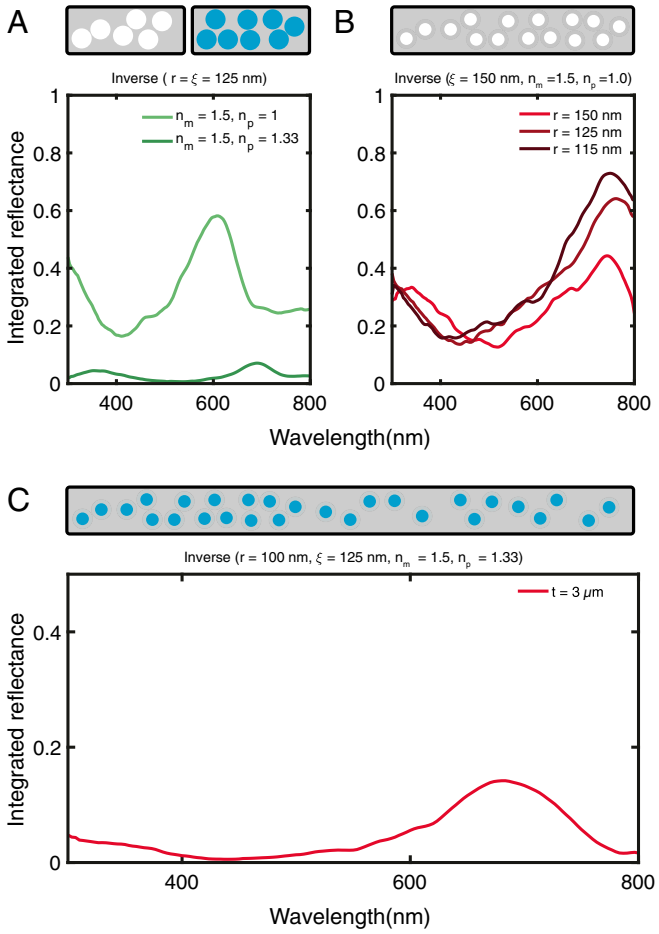

Fig. 3. Simulated optical response for inverse photonic glasses with advanced designs. (*A*) Effect of the refractive index of the scatters. Decreasing the refractive index contrast between scatterers and matrix leads to a broadband decrease of the reflectance, increasing the color purity. The simulated structures have a filling fraction of ff = 0.5. (*B*) Effect of core-shell correlation. Decreasing the size of the scatterers (*r*, core) maintaining a fixed center-to-center correlation distance (ξ, shell) leads to a blue shift of the secondary short wavelength peak, caused by Mie resonances. To allow for the same filling fraction for different core sizes, a filling fraction of ff = 0.4 was employed. (*C*) The approaches presented in *A* and *B* were combined, resulting in both a decrease of the broadband background and a blue shift of the secondary peak. All simulated structures have a thickness of $t = 3$ μm.

the blue region and broadens the structural peak at long wavelengths. Similarly, reducing the filling fraction in inverse PGs leads to a red shift of the structural peak, due to an increase of the effective refractive index of the system. In parallel, the relative intensity of the structural peak decreases compared to the Mie resonance at short wavelengths (*SI Appendix*, Fig. S3*C*). The result of these effects on the overall appearance of the system is further studied in Fig. 4.

Advanced Scatterer Morphologies. Our observations remain valid also for complex scatterer geometries. Previous works introduced the idea of using core-shell particles to disentangle the contributions of form- and structure-factor and achieve a separated peak in the long-wavelength spectral region (5, 22, 35, 36). Fig. 3*B* shows that reducing the scattering center (core) size while keeping the structural correlation length leads to an increase of the intensity and width of the long-wavelength (structural) peak. At the same time the short-wavelength contribution from Mie resonances shifts farther away into the UV. In Fig. 3*A* we showed that a lowered refractive index contrast can suppress multiple scattering, while a separation of the form- and structure-factor contributions is possible via core-shell particles (Fig. 3*B*). In Fig. 3*C* both approaches are combined, to achieve higher color purity and saturation by a well-separated peak in the long-wavelength part of the visible spectrum.

Color Saturation and Purity. To better quantify and assess the results in terms of color purity and saturation, the reflectance spectra of direct, inverse, and core-shell PGs are converted to color hues. Color purity can be defined as the normalized distance from the white point in a chromaticity diagram in respect to the red point (in case of red colors). Saturation quantifies how much the reflected intensity is distributed across the spectrum of different wavelengths. A mathematical definition as well as the details of the spectrum to color conversion is reported in *Materials and Methods*. In Fig. 4*A* the different systems for red color hues are plotted in the CIE color space chromaticity diagram (see *SI Appendix*, Table S1, for the *xy* values). In Fig. 4*B* the corresponding purity and saturation values are calculated. Interestingly, all of the inverse PGs show a higher color purity and saturation value than the direct PG's red hues reported in ref. 14. However, both the core-shell inverse structures as well as the low refractive index contrast (e.g., polymer filled with water) do not lead to a significant improvement compared to the standard inverse PG. Combining both approaches leads to improved purity and saturation values. Still, the achievable color purity and saturation values remain far from the ideal (RGB) red color.

Discussion

In summary, we demonstrated that photonic glasses have intrinsic limitations in achieving saturated red hues due to the interplay between structure-factor–related resonance and form-factor–related scattering and a multiple scattering background, reinforcing the hypothesis that isotropic structural coloration, while it can be easily achieved in the UV–blue spectral region, is challenging to obtain for larger wavelengths. In detail, we showed that inverse PGs increase color saturation and purity compared to their direct counterpart. This result is a consequence of an optical response where the structure factor contribution dominates over the form-factor scattering resonances. Furthermore, we showed that isotropic structural coloration occurs in a light propagation regime intermediate between diffusive and ballistic transport, where resonant ensemble properties (structure factor) are dominating over a multiple scattering background. We observe that high color purity and color saturation for red hues cannot be reached in isotropic short-range order structures, even in the case of advanced scatterer morphologies. Such results, therefore, indicate that natural system might have been forced to evolve alternative strategies for production of red coloration, such as multilayer or diamond structures (37, 38).

While combing different scattering approaches can help improve color purity and saturation in photonic glasses, they might be more challenging to realize in natural systems than simply combing different mechanisms, such as adding absorption. Once absorption is added, more pure and saturated colors can be achieved (8, 39). However, in synthetic systems, especially in the case of metallic nanoparticles (40), one might question the need of adding a structural component as it plays a redundant role in the overall visual response. In this context, we believe that approaches aimed at designing the scattering elements, making use of the interplay between absorption and scattering via Kramer–Kronig relations, might be more suitable to increase scattering in the red spectral region (41). Although most efforts to fabricate systems exhibiting isotropic structural colors focus on the self-assembly of colloidal particles (8), other promising approaches have recently been explored combining the purity and saturation advantages of coloration from ordered structures

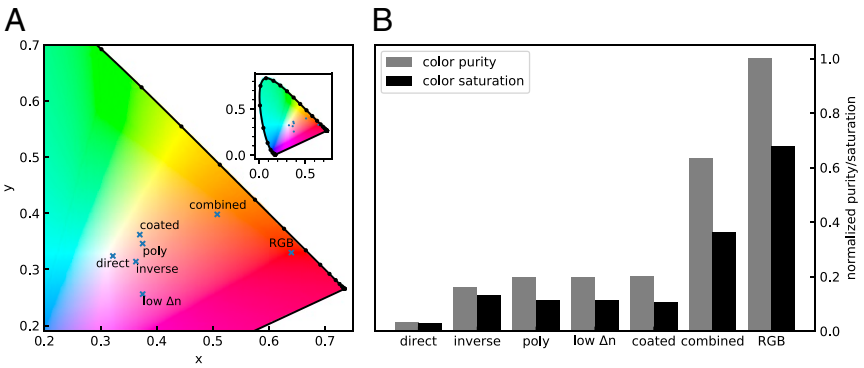

Fig. 4. Color purity and saturation. (*A*) Zoom-in to the CIE chromaticity diagram (inset). The *xy* values of the isotropic structural colors for various systems are displayed (see *SI Appendix* for values): direct, the ECPA multiple scattering model (see ref. 14 and *SI Appendix*, Fig. S3, $r = 128$ nm); inverse, an inverse PG with an isolated peak in the high-wavelength region (red curve in Fig. 2*B*); poly, the same structure with 20% polydispersity (dark red in *SI Appendix*, Fig. S3C); low Δn, an inverse PG with lowered refractive index contrast (dark green in Fig. 3*A*); coated, a core-shell inverse PG ($r = 115$ nm in Fig. 3*B*); and combined, a combined coated and lowered refractive index approach (Fig. 3C). For comparison, RGB red color is displayed (RGB). (*B*) The corresponding saturation and purity values.

with the morphological isotropy of spherical systems. In this context, block copolymers represent a promising candidate (42). Similarly, introducing disorder to ordered multilayer films gives rise to angle-independent structural coloration (12, 13). In conclusion, as convincing absorption-free, angle-independent, pure, and saturated red hues have not been obtained, we believe there is still space for further theoretical and experimental investigations to come up with strategies to produce viable alternatives to red pigments.

Materials and Methods

Numerical Calculations. To generate the 2D, disordered structures we used an inverse-design algorithm consisting of two steps (25): first, hard (nonoverlapping) particles are added using a random sequential approach until the desired filling fraction was reached, and second, the positions of these particles are gradually changed in order to minimize the difference between the targeted S(q) and the one of the structure. This code is available at the University of Cambridge data repository (https://doi.org/10.17863/CAM.54926).

To simulate the optical properities of the generated designed we used LUMERICAL 8.22 (Lumerical Solutions Inc.), a commercial-grade software using the FDTD method. Periodic boundaries conditions in the lateral direction, i.e., perpendicular to the incoming beam, Y and perfect matching layer boundaries in the X direction were used in all of the calculations. The excitation source was set as a plane wave. The simulations were performed in a purely 2D geometry, and their numerical stability/convergence was ensured by choosing an adequate simulation time and boundary conditions (assuring that the electric field in the structure decayed before the end of the calculation and that all of the excitation light was either reflected or transmitted). The 2D geometry of the simulations constrains light to a p-polarization (TM) state. This, however, does not represent a limitation for our study, as the scattering from isotropic, disordered systems is polarization-independent (43). Each of the presented curves was obtained averaging the optical simulations of seven different ensembles of particles with identical parameters.

Purity and Saturation of Color. To quantify color purity and saturation, reflection spectra are converted in color space coordinates assuming a standard observer (CIE 1931 2°) and a standard illuminant (Daylight D_{65}) (14, 25).

In particular, color purity can be calculated from

$$p_e = \sqrt{\frac{(x - x_n)^2 + (y - y_n)^2}{(x_l - x_n)^2 + (y_l - y_n)^2}}, \quad [1]$$

where x, y are the chromaticity coordinates in the xyY color space, with $x_n = 0.31271$, $y_n = 0.3290$ and $x_l = 0.64$, $y_l = 0.33$ being the coordinates of the white point and RGB red, respectively. Color saturation is calculated as

$$s_{ab} = \frac{C^*_{ab}}{L^*} = \frac{\sqrt{a^{*2} + b^{*2}}}{L^*}, \quad [2]$$

where L^* represents the lightness, and a^*, b^* are the chromaticity coordinates in CIELAB space.

Data Availability. All data needed to evaluate the conclusions in the paper are present in the paper and/or *SI Appendix* and/or available at the University of Cambridge data repository (https://doi.org/10.17863/CAM.54926) (44).

ACKNOWLEDGMENTS This work was supported in part by a Biotechnology and Biological Sciences Research Council David Phillips Fellowship (BB/K014617/1), the European Research Council (grant ERC-2014-STG H2020 639088), and the Swiss National Science Foundation under project P2ZHP2_183998.

1. P. Vukusic, J. Roy Sambles, Photonic structures in biology. *Nature* **424**, 852–855 (2003).
2. V. E. Johansen, O. D. Onelli, L. M. Steiner, S. Vignolini, *Photonics in Nature: From Order to Disorder* (Springer International Publishing, Cham, 2017).
3. M. Kolle *et al.*, Mimicking the colourful wing scale structure of the papilio blumei butterfly. *Nat. Nanotechnol.* **5**, 511–515 (2010).
4. J. D. Forster *et al.*, Biomimetic isotropic nanostructures for structural coloration. *Adv. Mater.* **22**, 2939–2944 (2010).
5. S. Magkiriadou, J.-G. Park, Y.-S. Kim, V. N. Manoharan, Disordered packings of core-shell particles with angle-independent structural colors. *Opt. Mater. Express* **2**, 1343–1352 (2012).
6. N. Vogel *et al.*, Color from hierarchy: Diverse optical properties of micron-sized spherical colloidal assemblies. *Proc. Natl. Acad. Sci. U.S.A.* **112**, 10845–10850 (2015).
7. H.-L. Liang *et al.*, Roll-to-roll fabrication of touch-responsive cellulose photonic laminates. *Nat. Commun.* **9**, 4632 (2018).
8. E. S. A. Goerlitzer, R. N. K. Taylor, N. Vogel, Bioinspired photonic pigments from colloidal self-assembly. *Adv. Mater.* **30**, 1706654 (2018).
9. L. Schertel *et al.*, Tunable high-index photonic glasses. *Phys. Rev. Materials* **3**, 015203 (2019).
10. Y. Wang *et al.*, Design, fabrication, and function of silk-based nanomaterials. *Adv. Funct. Mater.* **28**, 1805305 (2018).
11. B. Frka-Petesic, S. Vignolini, So much more than paper. *Nat. Photon.* **13**, 365–367 (2019).
12. D.-P. Song *et al.*, Photonic resins: Designing optical appearance via block copolymer self-assembly. *Macromolecules* **51**, 2395–2400 (2018).
13. C. L. C. Chan *et al.*, Visual appearance of chiral nematic cellulose-based photonic films: Angular and polarization independent color response with a twist. *Adv. Mater.* **31**, 1905151 (2019).
14. L. Schertel *et al.*, The structural colors of photonic glasses. *Adv. Optical Mate.* **7**, 1900442 (a2019).
15. S.-H. Kim *et al.*, Inverse photonic glasses by packing bidisperse hollow microspheres with uniform cores. *ACS Appl. Mater. Interfaces* **9**, 24155–24160 (2017).
16. R. O. Prum, R. H. Torres, S. Williamson, J. Dyck, Coherent light scattering by blue feather barbs. *Nature* **396**, 28–29 (1998).
17. R. O. Prum, R. Torres, C. Kovach, S. Williamson, S. M. Goodman, Coherent light scattering by nanostructured collagen arrays in the caruncles of the malagasy asities (eurylaimidae: Aves). *J. Exp. Biol.* **202**, 3507–3522 (1999).

18. R. O. Prum, R. Torres, Structural colouration of avian skin: Convergent evolution of coherently scattering dermal collagen arrays. *J. Exp. Biol.* **206**, 2409–2429 (2003).
19. V. Saranathan *et al.*, Structure and optical function of amorphous photonic nanostructures from avian feather barbs: A comparative small angle x-ray scattering (saxs) analysis of 230 bird species. *J. R. Soc. Interface* **9**, 2563–2580 (2012).
20. S. Kinoshita, *Structural Colors in the Realm of Nature* (World Scientific, 2008).
21. K. Sakoda, *Optical Properties of Photonic Crystals* (Springer Series in Optical Sciences, Springer, 2001).
22. S. Magkiriadou, J.-G. Park, Y.-S. Kim, V. N. Manoharan, Absence of red structural color in photonic glasses, bird feathers, and certain beetles. *Phys. Rev. E* **90**, 062302 (2014).
23. V. Hwang, A. B. Stephenson, S. Magkiriadou, J.-G. Park, V. N. Manoharan, Effects of multiple scattering on angle-independent structural color in disordered colloidal materials. *Phys. Rev. E* **101**, 012614 (2020).
24. E. R. Dufresne *et al.*, Self-assembly of amorphous biophotonic nanostructures by phase separation. *Soft Matter* **5**, 1792–1795 (2009).
25. G. Jacucci, J. Bertolotti, S. Vignolini, Role of anisotropy and refractive index in scattering and whiteness optimization. *Adv. Opt. Mater.* **7**, 1900980 (2019).
26. E. Abrahams, P. W. Anderson, D. C. Licciardello, T. V. Ramakrishnan, Scaling theory of localization: Absence of quantum diffusion in two dimensions. *Phys. Rev. Lett.* **42**, 673–676 (1979).
27. B. A. van Tiggelen, A. Lagendijk, D. S. Wiersma, Reflection and transmission of waves near the localization threshold. *Phys. Rev. Lett.* **84**, 4333–4336 (2000).
28. S. E. Skipetrov, B. A. van Tiggelen, Dynamics of Anderson localization in open 3D media. *Phys. Rev. Lett.* **96**, 043902 (2006).
29. A. Lagendijk, B. A. van Tiggelen, D. S. Wiersma, Fifty years of Anderson localization. *Phys. Today* **62**, 24–29 (2009).
30. S. E. Skipetrov, J. H. Page, Red light for Anderson localization. *New J. Phys.* **18**, 021001 (2016).
31. T. Sperling *et al.*, Can 3D light localization be reached in 'white paint'? *New J. Phys.* **18**, 013039 (2016).
32. L. S. Froufe-Pérez, M. Engel, J. J. Sáenz, S. Frank, Band gap formation and Anderson localization in disordered photonic materials with structural correlations. *Proc. Natl. Acad. Sci. U.S.A.* **114**, 9570–9574 (2017).
33. J. Haberko, L. S. Froufe-Pérez, F. Scheffold, Transition from light diffusion to localization in three-dimensional amorphous dielectric networks near the band edge. arXiv:1812.02095 (4 June 2020).
34. M. Russo *et al.*, Complete photonic band gaps in 3D foams. arXiv:1910.10039 (22 October 2019).
35. J.-G. Park *et al.*, Full-spectrum photonic pigments with non-iridescent structural colors through colloidal assembly. *Angew. Chem.* **126**, 2943–2947 (2014).
36. G. Shang *et al.*, Photonic glass for high contrast structural color. *Sci. Rep.* **8**, 7804 (2018).
37. A. E. Seago, P. Brady, J.-P. Vigneron, T. D. Schultz, Gold bugs and beyond: A review of iridescence and structural colour mechanisms in beetles (coleoptera). *J. R. Soc. Interface* **6** (suppl. 2), S165–S184 (2009).
38. B. D. Wilts, K. Michielsen, H. De Raedt, D. G. Stavenga, Sparkling feather reflections of a bird-of-paradise explained by finite-difference time-domain modeling. *Proc. Natl. Acad. Sci. U.S.A.* **111**, 4363–4368 (2014).
39. S.-H. Kim *et al.*, Solution-processable photonic inks of Mie-resonant hollow carbon–silica nanospheres. *Small* **15**, 1900931 (2019).
40. S.-J. Lee, S. Kumar, J. W. Choi, V. Y. Kim, J.-S. Lee, Copolymer particles with incorporated gold and silver nanoparticles to absorb short-wavelength scattering in full-color photonic glasses. *Part. Part. Syst. Char.* **36**, 1900167 (2019).
41. B. D. Wilts, W. Bas, H. L. Leertouwer, U. Steiner, D. G. Stavenga, Extreme refractive index wing scale beads containing dense pterin pigments cause the bright colors of pierid butterflies. *Adv. Optical Mater.* **5**, 1600879 (2017).
42. D.-P. Song, T. H. Zhao, G. Guidetti, S. Vignolini, R. M. Parker, Hierarchical photonic pigments via the confined self-assembly of bottlebrush block copolymers. *ACS Nano* **13**, 1764–1771 (2019).
43. E. Akkermans, G. Montambaux, *Mesoscopic Physics of Electrons and Photons* (Cambridge University Press, 2007).
44. L. Schertel *et al.*, Research data supporting "The limitations of extending nature's color palette in correlated, disordered systems." University of Cambridge data repository. https://doi.org/10.17863/CAM.54926. Deposited 10 July 2020.